

01 Jan 2010

## Theory of Breakup of Core Fluids Surrounded by a Wetting Annulus in Sinusoidally Constricted Capillary Channels

Igor A. Beresnev

Wen Deng

Missouri University of Science and Technology, wendeng@mst.edu

Follow this and additional works at: [https://scholarsmine.mst.edu/civarc\\_enveng\\_facwork](https://scholarsmine.mst.edu/civarc_enveng_facwork)



Part of the [Civil Engineering Commons](#)

---

### Recommended Citation

I. A. Beresnev and W. Deng, "Theory of Breakup of Core Fluids Surrounded by a Wetting Annulus in Sinusoidally Constricted Capillary Channels," *Physics of Fluids*, vol. 22, no. 1, American Institute of Physics (AIP), Jan 2010.

The definitive version is available at <https://doi.org/10.1063/1.3294887>

This Article - Journal is brought to you for free and open access by Scholars' Mine. It has been accepted for inclusion in Civil, Architectural and Environmental Engineering Faculty Research & Creative Works by an authorized administrator of Scholars' Mine. This work is protected by U. S. Copyright Law. Unauthorized use including reproduction for redistribution requires the permission of the copyright holder. For more information, please contact [scholarsmine@mst.edu](mailto:scholarsmine@mst.edu).

# Theory of breakup of core fluids surrounded by a wetting annulus in sinusoidally constricted capillary channels

Igor A. Beresnev<sup>a)</sup> and Wen Deng<sup>b)</sup>

Department of Geological and Atmospheric Sciences, Iowa State University,  
253 Science I, Ames, Iowa 50011-3212, USA

(Received 22 May 2009; accepted 22 December 2009; published online 21 January 2010)

Analysis of core-annular dynamics in the presence of base flow for arbitrary fluid viscosities leads to an equation describing the temporal evolution of the fluid/fluid interface. The equation follows from the conservation of mass in the “small-slope” approximation. Its useful applications occur, for example, in chemical engineering and petroleum recovery. The nonlinear equation allows inexpensive numerical analysis. For sinusoidally constricted pores, a purely geometric criterion exists that enables or prohibits the core-fluid breakup in the necks of the constrictions. The geometrically favoring condition sets up capillary-pressure gradients that ensure a continuous outflow of the core fluid from the necks into the “crests” of the profile. Such behavior is indeed observed in the numerical solutions of the evolution equation. For relatively large slopes of the initial configuration, setting up larger pressure gradients, the interface shape remains “smooth,” the evolution times are relatively fast, and the breakup is typically achieved by the growing film-fluid collar touching the axis of the channel at a single point. No satellite droplets are produced. Decreasing the slope lengthens the evolution times, allowing the formation and growth of “wavy” disturbances on the initial interface profile, which may touch the axis of the capillary in several places forming satellite drops. Thinner initial annuli also slow down the evolution process. Instability develops for the cases of the core both more and less viscous than the film. Finally, if the geometry prohibits the snap-off altogether, the initial interface configurations decay into steady-state solutions, and no breakup takes place. The solutions of the evolution equation validate well against two computational-fluid-dynamics codes. © 2010 American Institute of Physics.  
[doi:10.1063/1.3294887]

## I. INTRODUCTION

Evolution equations have been often used to describe the temporal dynamics of free fluid/fluid interfaces, e.g., Refs. 1 (Sec. 60, problem 4) and 2–5. The advantage of this approach is that it reduces the hydrodynamic problem to a single partial-differential equation that is much easier to solve numerically than the original full system of equations of two-phase fluid dynamics, e.g., Refs. 6 and 7.

Hammond<sup>3</sup> derived a nonlinear evolution equation for the thickness of a thin film of a wetting fluid adsorbed on the wall of a cylindrical capillary. The equation was based on the assumption of an inviscid, nonwetting core filling the middle of the channel, within which constant zero pressure was postulated [Ref. 3, Eqs. (3.3)–(3.7)]. This assumption allowed the introduction of scaled variables [Ref. 3, Eqs. (3.12)–(3.15)] that made the approximations leading to the evolution equation possible. The analysis was strictly applicable to an inviscid core only.

Gauglitz and Radke<sup>4</sup> subsequently showed that Hammond’s<sup>3</sup> *thin-film* approximation suffered from inaccurate representation of the fluid/fluid interfacial curvature, which led to incorrect prediction of the interface dynamics; they proposed an extended, more accurate evolution equa-

tion, which was called the *small-slope* one. The analysis still dealt with a straight cylindrical channel. Gauglitz and Radke,<sup>5</sup> however, generalized this approach to the case of a sinusoidally constricted capillary tube. The generalized small-slope equation was applied to the description of a breakup of gas bubbles surrounded by water: the evolution of the wetting film was followed until the latter formed bridges (collars) across the tube. Constant zero pressure in the internal (gas) phase was again postulated (Ref. 5, p. 39).

One can see that previous work has dealt with the evolution equations for the thickness of wetting films inside capillaries in the presence of zero-pressure, inviscid internal phase. What made both Hammond and Gauglitz and Radke’s derivations possible was the latter assumption, which allowed the use of explicit expressions for the absolute pressure in the film based on the interface curvature [Ref. 3, Eqs. (3.3) and (3.4); Ref. 4, Eqs. (6) and (7); and Ref. 5, Eqs. (13), (17), and (18)]. The pressure field in the film was thereby fully defined. If the core were viscous, this would not be the case, as the assumption of constant pressure in the core would no longer be valid, and Laplace’s law would only provide a relative pressure difference between the two fluids. The absolute pressure in neither phase would be known, preventing the development of an evolution equation. This difficulty was not overcome in the studies by Papageorgiou *et al.*,<sup>8</sup> Kerchman,<sup>9</sup> and Wei and Rumschitzki,<sup>10,11</sup> who virtually repeated Hammond’s analysis using the same assump-

<sup>a)</sup>Telephone: 515-294-7529. Fax: 515-294-6049. Electronic mail: beresnev@iastate.edu.

<sup>b)</sup>Electronic mail: deng@iastate.edu.

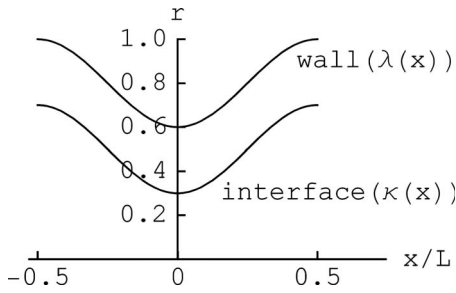


FIG. 1. Geometry of the problem.

tions and the same scaling scheme. As Hammond's model, neither predicted the formation of bridges as well. In general, the inherent inability of the perturbation analyses, based on the thin-film approximation, to predict the formation of liquid bridges,<sup>3,8-11</sup> limits their practical usefulness and is a significant shortcoming. On the other hand, the small-slope approximation, applied to a spontaneous breakup, not only captures the formation of bridges but, for the case of gas bubbles in capillaries, leads to excellent agreement with the experiment.<sup>5</sup>

No theory therefore still exists that would describe the evolution of an interface for the case of arbitrary viscosities and thicknesses of the fluids in the wetting annulus and the core. Our goal is to develop and analyze such an evolution equation, in the small-slope approximation and the presence of base flow, identifying the conditions under which the core fluid filling corrugated channels can break up into isolated drops. Problems of this type occur, for example, in chemical engineering and petroleum recovery. Keeping in mind this practical relevance, we will identify the capillary tube with a "pore."

Applications to pore geometries will allow us to neglect gravity effects. The ratio of gravitational to capillary forces is controlled by the Bond number,  $Bo = \Delta\rho g d^2 / \sigma$ , where  $\Delta\rho$  is the density difference between the film and core fluids,  $g$  is the acceleration of gravity,  $d$  is the characteristic pore diameter, and  $\sigma$  is the interfacial tension. Even for the typical maximum pore diameters of 100  $\mu\text{m}$  and maximum density differences of  $\approx 1000 \text{ kg/m}^3$ , assuming a characteristic surface tension of 0.040 N/m, we obtain  $Bo \approx 10^{-3}$ , which illustrates the dominance of capillary effects. The same conclusion was reached by Hammond (Ref. 3, p. 364).

Our analysis will also assume the smallness of capillary numbers or the dominance of capillary forces over viscous ones. Such an assumption, for example, is well justified in oil-recovery operations, which are characterized by capillary numbers on the order of  $10^{-6}$ – $10^{-8}$ , e.g., Ref. 12 (p. 58).

## II. THE EVOLUTION EQUATION OF THE FLUID/FLUID INTERFACE

The geometry of the problem is illustrated in Fig. 1, where an axisymmetric pore channel with sinusoidal profile is depicted in the cylindrical coordinate system with a fluid/fluid interface inside. The indices "1" and "2" will designate the variables in the core fluid and the wetting annulus, respectively. Following Gauglitz and Radke (Ref. 5, p. 16) and

keeping the same notation, we introduce the problem variables and nondimensionalize them as follows:

$$r = r^*/R_T^*, \quad x = x^*/R_T^*, \quad \tau = t^*/(\mu_1^* R_T^*/\sigma^*), \quad (1)$$

$$p = p^*/(\sigma^*/R_T^*), \quad Q = Q^*/(\sigma^* R_T^{*2}/\mu_1^*).$$

Here  $r^*$  and  $x^*$  are the radial and axial coordinates, respectively,  $t^*$  is the time,  $p^*$  is the pressure,  $Q^*$  is the volumetric flow rate,  $R_T^*$  is the maximum radius of the tube, and  $\mu_1^*$  is the core dynamic viscosity. The "asterisks" will always indicate the dimensional variables, and their "nonasterisked" counterparts will be the nondimensional ones.

The shape of the pore wall is represented by a sinusoidal function

$$r|_{\text{wall}} \equiv \lambda(x) = 1 - a \left( 1 + \cos 2\pi \frac{x}{2/\alpha} \right), \quad (2)$$

which has the wavelength of  $L \equiv 2/\alpha$ ; the parameters  $a$  and  $\alpha$  conveniently characterize the minimum radius of the pore  $(1-2a)$  (the radius at the neck of the constriction) and the slope of the wall, respectively. The slope parameter  $\alpha$  has a simple geometric meaning: it is the ratio of the maximum radius of the channel to half of its wavelength,  $\alpha = R_T^*/(L^*/2)$ . The dimensionless function (2), labeled the "wall," is plotted in Fig. 1.

The radial position of the fluid/fluid interface is represented by the dimensionless  $r|_{\text{interface}} \equiv \kappa(x)$ . From Laplace's law,

$$p_c^* \equiv p_1^* - p_2^* = \sigma^* K^*, \quad (3)$$

where  $K^*$  is the mean curvature of the fluid surface  $\kappa(x^*)$  and  $p_c^*$  is the "capillary pressure." The assumption of small capillary numbers allows us to neglect the contribution of viscous stresses to the boundary condition (3), e.g., Ref. 13 (p. 59). As seen from Eq. (3), the determination of pressures requires an expression for the curvature of an axisymmetric surface in cylindrical coordinates. Such an expression is given, for example, by Atherton and Homsy (Ref. 2, p. 76) or De Gennes *et al.* [Ref. 14, Eq. (1.14)] and also was derived by Beresnev *et al.*<sup>15</sup> from the general equations of differential geometry. In dimensionless form, the exact equation (3) for the pressure difference across the interface becomes {cf. the capillary-pressure term in Ref. 5 [Eq. (B5)] given without derivation}

$$p_1 - p_2 = \frac{1}{\kappa \left[ 1 + \left( \frac{\partial \kappa}{\partial x} \right)^2 \right]^{1/2}} - \frac{\frac{\partial^2 \kappa}{\partial x^2}}{\left[ 1 + \left( \frac{\partial \kappa}{\partial x} \right)^2 \right]^{3/2}}. \quad (4)$$

The sign of the second term in Eq. (4) has been chosen to correctly represent an increase in the capillary pressure under the "convex" part of the interface. Indeed, under the "crest" of the sinusoidal profile (having the maximum radius of 1 in Fig. 1), the two mutually orthogonal normal cross sections of the interface (one in the plane of Fig. 1 and one perpendicular to it) are convex; both terms in the right-hand side of Eq. (4) must then be positive. The first term is always positive. To check if the sign of the second term is correct,

we take, for example, an interface that follows the shape of the wall [Eq. (2)]. The second derivative of Eq. (2) is  $\pi^2 \alpha^2 a \cos 2\pi(x/2/\alpha)$ , which is negative at the crest (e.g.,  $x=1/\alpha$ ). This provides the correct positive sign of the second term in Eq. (4).

The evolution equation is derived as the mathematical expression of the conservation of mass. The volume of the core segment with radius  $R_T^* \kappa$  and length  $dx^*$  is  $\pi(R_T^* \kappa)^2 dx^*$ , and the rate of the volume change is  $2\pi R_T^{*2} \kappa (\partial \kappa / \partial t^*) dx^*$ . Conservation of mass relates this rate of change to the differential of the volume flux in the core  $dQ_1^*$  as  $(\partial Q_1^* / \partial x^*) dx^* = -2\pi R_T^{*2} \kappa (\partial \kappa / \partial t^*) dx^*$ . Nondimensionalizing according to Eq. (1) yields

$$\frac{\partial \kappa}{\partial \tau} = -\frac{1}{2\pi \kappa} \frac{\partial Q_1}{\partial x}. \quad (5)$$

To close the equation, one needs to explicitly express the volume flux in the core  $Q_1$  through the interface position  $\kappa$ . With the small-slope assumption, such as by Gauglitz and Radke,<sup>4,5</sup> the fluid flow in the core and the annulus can locally be approximated as Poiseuille flow. In adopting this approximation, we therefore assume the smallness of the Reynolds number (Re). The exact axisymmetric solution of the stationary Navier–Stokes equation is known, which, when applied to the core-annular geometry, results in an analytical expression for the steady-state Poiseuille flow in the core and the annulus (Ref. 13, Sec. 2-1). However, this solution assumes an equal pressure gradient in both fluid phases. Since, by nature of our problem, we are interested in the capillary flow to which Laplace’s law applies, the local pressure gradients in the core and the annulus will generally be different. We therefore need to rederive the core-annular Poiseuille flow for the general case of nonequal pressure gradients in the two fluids.

Let local pressure gradients be  $p_{1x}^* \equiv \partial p_1^* / \partial x^*$  and  $p_{2x}^* \equiv \partial p_2^* / \partial x^*$ . Developing the solution of the Navier–Stokes equation for the cylindrical core-annular geometry for the case of  $p_{1x}^*$  nonequal to  $p_{2x}^*$  leads to the expressions for the axial velocities  $u_1^*$  and  $u_2^*$ ,

$$u_1^*(r^*) = \frac{p_{1x}^*}{4\mu_1^*} (r^{*2} - R_1^{*2}) + \frac{p_{2x}^*}{4\mu_2^*} (R_1^{*2} - R_2^{*2}) + \frac{R_1^{*2}}{2\mu_2^*} (p_{1x}^* - p_{2x}^*) \ln \frac{R_1^*}{R_2^*}, \quad (6a)$$

$$u_2^*(r^*) = \frac{p_{2x}^*}{4\mu_2^*} (r^{*2} - R_2^{*2}) + \frac{R_1^{*2}}{2\mu_2^*} (p_{1x}^* - p_{2x}^*) \ln \frac{r^*}{R_2^*}, \quad (6b)$$

where  $R_1^*$  and  $R_2^*$  are the radius of the core and the external radius of the tube, respectively. It is easy to check that these expressions reduce to the known velocities for equal gradients  $p_{1x}^* = p_{2x}^*$  [Ref. 13, Eqs. (2-1.9) and (2-1.10)]. Integration of the velocity profiles (6) gives the respective volume fluxes in the core and the annulus,

$$Q_1^* = 2\pi \int_0^{R_1^*} u_1^* r^* dr^* = \frac{\pi}{2} R_1^{*2} \left[ -\frac{p_{1x}^*}{4\mu_1^*} R_1^{*2} + \frac{p_{2x}^*}{2\mu_2^*} (R_1^{*2} - R_2^{*2}) + \frac{R_1^{*2}}{\mu_2^*} \ln \frac{R_1^*}{R_2^*} (p_{1x}^* - p_{2x}^*) \right], \quad (7a)$$

$$Q_2^* = 2\pi \int_{R_1^*}^{R_2^*} u_2^* r^* dr^* = -\frac{\pi p_{2x}^*}{8\mu_2^*} (R_1^{*2} - R_2^{*2})^2 - \frac{\pi R_1^{*2} R_2^{*2}}{2\mu_2^*} (p_{1x}^* - p_{2x}^*) \left( \frac{1}{2} + \frac{R_1^{*2}}{R_2^{*2}} \ln \frac{R_1^*}{\sqrt{e} R_2^*} \right), \quad (7b)$$

where  $e$  is the base of the natural logarithm.

After nondimensionalization, expression (7a) for  $Q_1$  can be substituted into Eq. (5). However, the pressure gradients  $p_{1x}$  and  $p_{2x}$  will still be undetermined and need to be expressed through the interface position  $\kappa$  to close the evolution equation. This is achieved as follows.

Laplace’s law (4) relates  $p_1$  and  $p_2$ . The small-slope approximation allows us to neglect the derivative terms in the brackets in Eq. (4), i.e.,  $\partial \kappa / \partial x \ll 1$ . Since these terms are squared, the approximation should remain reasonable even if the condition is relaxed to  $\partial \kappa / \partial x < 1$ . If the core initially follows the shape of the wall, by taking the derivative of Eq. (2) this condition can be seen to be equivalent to  $\alpha < 1$ . We will use the latter as the condition for the small-slope approximation. It, of course, has a transparent geometric meaning,  $R_T^* < L^*/2$ .

The small-slope approximation is the better the smaller the parameter  $\alpha$  is. As long as it remains valid, the locally Poiseuille approximations for the flow in both the core and the annulus ( $Q_1$  and  $Q_2$ , respectively), which fully take viscosities into account, remain applicable too. The limits of validity of this analysis can only be verified through an experiment or computational fluid dynamics (CFD); we take the latter approach in the final section of the paper.

Equation (4) for the pressure difference across the interface then simplifies to

$$p_1 - p_2 = \frac{1}{\kappa} - \frac{\partial^2 \kappa}{\partial x^2}, \quad (8)$$

or, by differentiating,

$$p_{1x} = p_{2x} - \frac{1}{\kappa^2} \frac{\partial \kappa}{\partial x} - \frac{\partial^3 \kappa}{\partial x^3}. \quad (9)$$

Continuity requires that

$$Q_1 + Q_2 = Q, \quad (10)$$

where  $Q$  is the constant total volumetric flow rate in the tube. Equations (9) and (10), with Eq. (7) in mind, represent a

system of two algebraic equations with two unknowns  $p_{1x}$  and  $p_{2x}$ . Solving for them and substituting the solution for  $p_{1x}$  into the nondimensionalized  $Q_1$  in Eq. (7a), and then using the result in Eq. (5), closes the evolution equation de-

fining the radial position of the interface, which includes the effect of the imposed base flow with constant rate  $Q$  and arbitrary viscosities of the fluids. With the intervening algebra omitted, the equation is

$$\frac{\partial \kappa}{\partial \tau} = -\frac{1}{2\pi} \frac{\mu_2 Q}{\mu_1 \kappa} \frac{\partial}{\partial x} \left[ \frac{1 + \frac{2\mu_1}{\mu_2} \left( \frac{\lambda^2}{\kappa^2} - 1 \right)}{\frac{\lambda^4}{\kappa^4} + \frac{\mu_2}{\mu_1} - 1} \right] + \frac{1}{4\kappa} \frac{\partial}{\partial x} \left( \kappa^2 \left( \frac{\partial \kappa}{\partial x} + \kappa^2 \frac{\partial^3 \kappa}{\partial x^3} \right) \left\{ \frac{\left( \frac{\lambda^2}{\kappa^2} - 1 \right) \left[ \left( \frac{\mu_1}{\mu_2} - \frac{1}{4} \right) \frac{\lambda^2}{\kappa^2} + \frac{3}{4} - \frac{\mu_1}{\mu_2} \right]}{\frac{\lambda^4}{\kappa^4} + \frac{\mu_2}{\mu_1} - 1} - \frac{\mu_1}{\mu_2} \ln \frac{\lambda}{\kappa} \right\} \right). \quad (11)$$

Note that Kouris and Tsamopoulos<sup>16</sup> performed a computational-fluid-dynamics study of the interface dynamics in a core-annular flow of two viscous fluids in a channel with sinusoidal cross section. The interface evolution has not led to the breakup or the formation of satellite droplets. As for Hammond's<sup>3</sup> study, this lack of the formation of bridges can be traced back to an insufficient approximation of the interfacial curvature. The undervaluation of the second-derivative term in the Kouris and Tsamopoulos analysis can be ascertained by comparing the curvature term in Eq. (15) in their paper with Eq. (8) above. As a result, both the fluid snap-off and the production of satellite droplets naturally appear in our analysis. In a follow-up numerical study, Kouris and Tsamopoulos<sup>7</sup> removed the restrictions on representing the interfacial curvature, which led to their documenting a complete core-fluid breakup as well.

Equation (11) is a nonlinear evolution equation of fourth order describing the dynamics of the free interface. Its solutions will be investigated numerically in Sec. III. For validation and comparison, we will also present the computational-fluid-dynamics simulations of the same scenarios.

### III. INTERFACE DYNAMICS AS THE SOLUTION OF THE EVOLUTION EQUATION

#### A. The linear stability analysis

We start with a linear stability analysis of Eq. (11). Representing the initial interface configuration as  $\kappa = \kappa_0 (1 + \beta e^{\eta t + ikx})$ , where  $\beta \ll 1$ , and linearizing (setting  $1/\kappa \approx 1/\kappa_0$ ,  $\kappa^2 \approx \kappa_0^2$ ,  $\kappa^4 \approx \kappa_0^4$ , and  $\lambda = 1$ ), we obtain, upon substitution into Eq. (11),

$$\eta = \frac{\kappa_0 k^2}{4} (\kappa_0^2 k^2 - 1) \times \left\{ \frac{\left( \frac{1}{\kappa_0^2} - 1 \right) \left[ \left( \frac{\mu_1}{\mu_2} - \frac{1}{4} \right) \frac{1}{\kappa_0^2} + \frac{3}{4} - \frac{\mu_1}{\mu_2} \right]}{\frac{1}{\kappa_0^4} + \frac{\mu_2}{\mu_1} - 1} + \frac{\mu_1}{\mu_2} \ln \kappa_0 \right\}. \quad (12)$$

Taking the derivative  $\eta'(k)$  and equating it to zero, we find

that  $\eta$  takes the maximum positive value at the wave number  $k_{\max} = 1/(\sqrt{2}\kappa_0)$ . Since  $k = 2\pi/l$ , where  $l$  is the wavelength of the surface disturbance, the wavelength  $l_{\max}$ , corresponding to  $k_{\max}$ , becomes  $2^{3/2}\pi\kappa_0$ . We thus recover the result of Hammond's linear stability analysis for the fastest-growing wavelength for all realistic core viscosities [Ref. 3, Eqs. (2.23) and (2.24) and p. 369]. Consistency with Hammond's result is understood from the fact that he also used the Stokes (small-Reynolds-number) approximation, albeit without an imposed flow.

Also, it can be directly verified that the expression in the curly braces in Eq. (12) is always negative. The condition for  $\eta$  to stay positive (the condition for the disturbance to grow) is consequently  $\kappa_0^2 k^2 < 1$  or  $l > 2\pi\kappa_0$ . This recovers the expression for the wavelengths of surface disturbances that cause the Plateau-Rayleigh instability (disintegration) of a liquid cylinder of radius  $\kappa_0$  [Ref. 14, Eq. (5.22)].

The linear stability analysis therefore verifies that our evolution equation correctly reduces to known asymptotic cases.

#### B. Geometric condition for core-fluid breakup

A purely geometric condition exists for the core fluid's snap-off in the necks of the constrictions.<sup>15</sup> This condition can be derived exactly for the case of pure surface-tension-driven flow (no base flow). Consider capillary pressures in the neck  $p_c^{\text{neck}}$  and the crest  $p_c^{\text{crest}}$  of the profile, which, from Eq. (3), are controlled by the geometry only. Let us conjecture that the breakup of the core fluid is governed by the geometric condition  $p_c^{\text{neck}} > p_c^{\text{crest}}$ . For the surface-tension-driven flow, only three combinations, relating the pressures in the annulus and core fluids in the crests and the necks, can physically exist,

$$\begin{aligned} p_1^{\text{neck}} &< p_1^{\text{crest}} \\ p_2^{\text{neck}} &> p_2^{\text{crest}}, \end{aligned} \quad (13a)$$

$$\begin{aligned} p_1^{\text{neck}} &= p_1^{\text{crest}} \\ p_2^{\text{neck}} &= p_2^{\text{crest}}, \end{aligned} \quad (13b)$$

$$\begin{aligned} p_1^{\text{neck}} &> p_1^{\text{crest}} \\ p_2^{\text{neck}} &< p_2^{\text{crest}} \end{aligned} \quad (13c)$$

Equation (13) simply asserts the conservation of mass: e.g., if there is an inflow of the core fluid into the neck, there must be a respective outflow of the film fluid from the neck [Eq. (13a)], and so forth. Subtracting the second inequality from the first in Eq. (13a) keeps the  $<$  sign true, so we obtain, from the definition in Eq. (3),  $p_c^{\text{neck}} < p_c^{\text{crest}}$ , which contradicts the initial conjecture. Repeating the process for the equalities in Eq. (13b) again leads to a contradiction. The only combination compatible with the initial conjecture  $p_c^{\text{neck}} > p_c^{\text{crest}}$  is Eq. (13c); however, the latter implies the outflow of the core phase from the necks into the crests ( $p_1^{\text{neck}} > p_1^{\text{crest}}$ ) accompanied by the invasion of the film fluid into the neck  $p_2^{\text{neck}} < p_2^{\text{crest}}$  with a formation of a bridge across the tube. We have thus proved that the geometric condition  $p_c^{\text{neck}} > p_c^{\text{crest}}$  is the condition for the initiation of the breakup process that may lead to the pinch-off of the core.

This condition can be formulated explicitly. Suppose, for simplicity, that the initial interface follows the shape of the wall,  $\kappa(x) = \lambda(x) - b$ , where  $b$  is a constant. Then, from Eqs. (2) and (4), capillary pressure  $p_c$  at the crests of the interface profile is  $p_c^{\text{crest}} = 1/R_{\text{max}} + \pi^2 \alpha^2 a$ , and the pressure at the “troughs” (the necks of the constrictions) is  $p_c^{\text{neck}} = 1/R_{\text{min}} - \pi^2 \alpha^2 a$ , where  $R_{\text{min}} = 1 - 2a - b$  and  $R_{\text{max}} = 1 - b$  are the minimum and the maximum radii of the interface profile. The pinch-off condition  $p_c^{\text{neck}} > p_c^{\text{crest}}$  is then reformulated as

$$\alpha < \frac{1}{\pi \sqrt{R_{\text{min}} R_{\text{max}}}}. \quad (14)$$

Condition (14) was first deduced by Beresnev *et al.* [Ref. 15, Eq. (6)] based on more general qualitative reasoning that did not preclude the presence of base flow. A review of published numerical and experimental observations of core-phase breakup in sinusoidal channels supported the validity of this purely geometric criterion. It is also worthwhile noting that all tube geometries used in the computational-fluid-dynamics simulation by Kouris and Tsamopoulos<sup>7</sup> satisfied geometric condition (14) as well.

Note that this “static” criterion does not take the dynamics of the interface into account and strictly applies to the initiation of the breakup only. However, when the core fluid starts flowing out of the neck, with the interface there moving toward the axis of the pore, the radius  $R_{\text{min}}$  progressively tends to zero, while  $R_{\text{max}}$  remains by order of magnitude the same. Condition (14), therefore, if satisfied, can be expected to be sufficient to complete the snap-off.<sup>15</sup> We will verify this observation from the numerical investigation of the evolution equation.

Also note that in the limiting case of  $R_{\text{min}} = R_{\text{max}} = R$ , Eq. (14) reduces to  $L > 2\pi R$ , which again recovers the condition for the Plateau-Rayleigh instability.

## C. Numerical solution of the evolution equation and validation against CFD

### 1. Algorithm descriptions

Equation (11) was solved numerically using the computational package MATHEMATICA<sup>®</sup> to the precision of six decimal digits. The adaptive “method of lines” is used to solve the partial differential equation represented by Eq. (11). To advance the solution to the next time level, the spatial derivatives [the right-hand side of Eq. (11)] are first calculated, leading to a first-order ordinary differential equation in time at every node of the spatial grid. The resulting  $N$  ordinary differential equations ( $N$  is the number of nodes) are then solved as an initial-value problem at every node to advance the solution one step in time. The spatial derivatives are then recalculated and the process is repeated.

The wall and the initial-interface configurations used in the first example are shown in Fig. 1. To avoid artificial reflections from the ends of the  $x$ -domain, the periodic boundary condition was used:  $\kappa(\tau, -L/2) = \kappa(\tau, L/2)$ . The evolution of the fluid/fluid interface was computed until the latter reached the centerline (axis) of the pore ( $r=0$ ). Since the condition for the core fluid breakup appears to be controlled by inequality (14), cases were investigated in which this inequality was and was not satisfied, keeping parameter  $\alpha$  small enough to remain within the limits of the small-slope approximation.

We use a uniform film thickness as an initial configuration. If the core phase were a gas bubble in a straight cylindrical tube, a steady-state film thickness would be a fraction of the tube radius proportional to the positive power of the capillary number.<sup>17</sup> However, the initial condition in our study should rather be representative of the sinusoidal geometry, in which the local capillary number varies with the fluid velocity, being greater where the channel’s radius is small than where it is large. This dependence will tend to equalize the film thickness along the sinusoidal pore. In the laboratory experiments we currently conduct, we indeed observe that the thickness of the wetting annulus, left behind by the invasion of a viscous core fluid into a wetting-fluid-filled sinusoidal channel, is visually constant. For the absence of a better model, we choose a uniform thickness as an appropriate initial condition in the examples we provide.

Mimicking a typical oil-recovery application, assuming a water viscosity of 0.001 Pa s and a typical oil viscosity of 0.01 Pa s (Ref. 18, Fig. A-2), the ratio of  $\mu_1/\mu_2$  in all cases except one (Fig. 7) was set to 10. In keeping with the same application, we should obtain an upper bound on the flow rate  $Q$  expected for a porous channel in an oil reservoir. Assuming water as the reservoir’s most abundant phase, we can obtain from Darcy’s law  $Q_D^* = (k^* A^* / \mu_w^*) p_{x^*}$ , where  $k^*$  is the permeability,  $\mu_w^*$  is water viscosity,  $A^*$  is the cross-sectional area, and  $p_{x^*}$  is the background pressure gradient. To convert  $Q_D^*$  to an estimate of the velocity in a single channel, we divide it by the fraction of the area occupied by the pores,  $u^* = (k^* / \varphi \mu_w^*) p_{x^*}$ , where  $\varphi$  is the porosity. For a channel with a characteristic radius  $R_T^*$ , the channel’s base-flow rate is then calculated as  $Q^* = \pi R_T^{*2} u^*$ . Nondimensionalizing according to Eq. (1) leads to  $Q = \pi k^* \mu_1 p_{x^*}^* / \varphi \sigma^* \mu_w^*$ . The

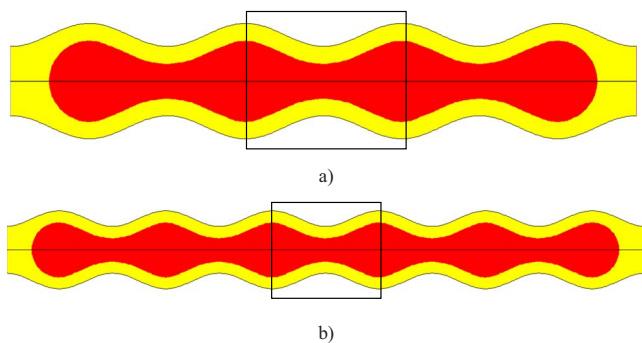


FIG. 2. (Color online) (a) Four periods and (b) six periods of the computational domain for the CFD simulations.

oil-field maximum pressure gradients are on the order of  $10^6$  Pa/m, and the high end of reservoir permeabilities is  $10^{-11}$  m<sup>2</sup> (Ref. 19, Table 5.5.1). For the porosity of 0.25, taking the ratio of oil-to-water viscosities of 10 and the surface tension of 0.040 N/m results in  $Q=3 \times 10^{-2}$ . For a range of scenarios, we will use this upper-bound estimate as the value of  $Q$  in one example and will reduce it by a factor of 30 to  $Q=10^{-3}$  in another example. The respective capillary numbers,  $Ca = \mu_w^* u^* / \sigma^* = (\mu_w^* / \sigma^*) (Q^* / \pi R_T^{*2}) = Q \mu_w^* / \pi \mu_1^*$ , become  $10^{-3}$  and  $3 \times 10^{-5}$ .

The numerical solutions of the evolution equation are validated using the commercial finite-volume computational-fluid-dynamics code FLUENT. The simulations were run in FLUENT's volume of fluid (VOF) axisymmetric model for the immiscible multiphase flow. The mesh-generation software GAMBIT was used to construct the grid on which the axial and radial momentum, continuity, and volume-fraction equations were solved. A triangular mesh was generated, because we had found that simulations would be sensitive to the aspect ratio if a rectangular mesh was used. The following solution schemes for the VOF model were applied: the pressure staggering option for pressure interpolation, the second-order discretization for the volume-fraction equation, the pressure implicit with splitting of operators scheme for pressure-velocity coupling, and the second-order upwind discretization for the momentum equations. The computational domain comprised either four or six periods of the sinusoidal channel with a body of the core fluid inserted in the suspending fluid (Fig. 2) to match the preset initial configuration in the middle period of the channel (boxes in Fig. 2). The constant total flow rate was maintained. The middle period was used for the comparison to the theoretical calculations. The density and viscosity of the core fluid were 1000 kg/m<sup>3</sup> and 0.01 Pa s, and those in the film were 1000 kg/m<sup>3</sup> and 0.001 Pa s. The surface tension was set to 0.040 N/m. The tube had the maximum and minimum radii of 25 and 15  $\mu$ m, respectively; the initial film thicknesses were 7.5 and 3.75  $\mu$ m for the geometries of the two examples in Figs. 1 and 8, respectively.

Grid-refinement studies were performed to ensure that the computed profiles and times to breakup were grid independent. The typical results, obtained for the FLUENT simulations corresponding to Fig. 3(a), are summarized in Table I. Independence of the computed times to breakup has been

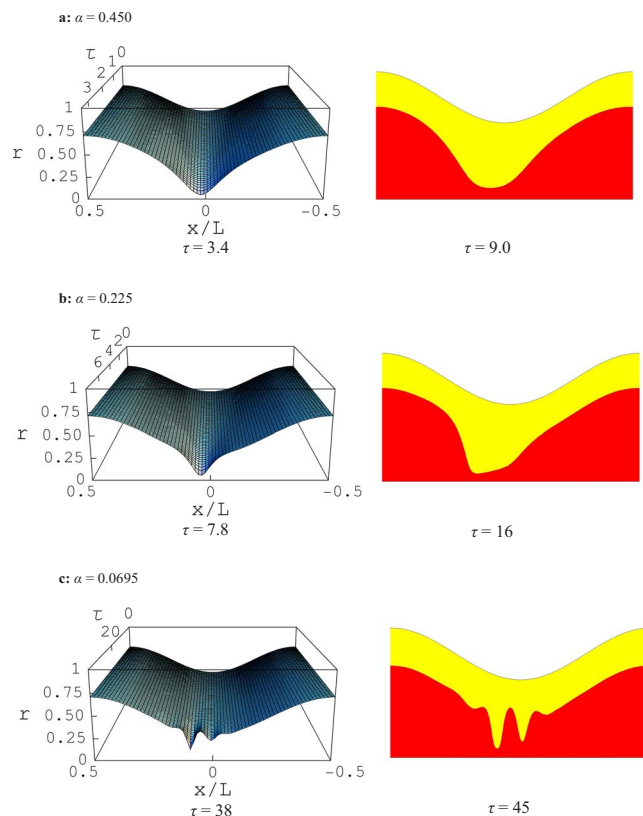


FIG. 3. (Color online) Temporal evolution of the initial interface profile with  $Q=3 \times 10^{-2}$  and increasing spatial periods of the sinusoidal wall.  $\mu_1/\mu_2=10$ . The results obtained through numerical integration of the evolution equation are shown on the left, and FLUENT results are on the right. The final dimensionless times are indicated under each plot. (a) The period of the fastest-growing disturbance of the linear stability analysis,  $\alpha=0.450$ , (b)  $\alpha=0.225$ , and (c)  $\alpha=0.0695$ .

ensured through the second digit. The results that will be presented are for the finest grid.

The advantage of using the evolution equation to calculate the dynamics of the interface can be illustrated as follows. Most runs required no more than several minutes to execute on a modern personal computer, while two-phase computations for same geometries in FLUENT took approximately 1 day per scenario.

For further verification, the same simulations were performed using another commercial CFD code COMSOL. It was chosen because FLUENT and COMSOL were based on totally different approaches to discretizing the governing equations and tracking the position of the free interface, providing independent control. While FLUENT uses the finite-volume method for the discretization and the volume-of-fluid method for resolving a moving interface, COMSOL implements the finite-element and the level-set methods, respectively.

TABLE I. Grid-refinement studies: the geometry as in Fig. 3(a).

	Mesh1	Mesh2	Mesh3
	8712 cells	35 674 cells	80 212 cells
Breakup time (s)	$6.55 \times 10^{-5}$	$6.76 \times 10^{-5}$	$6.78 \times 10^{-5}$

## 2. Results

The typical cases are presented as follows. We start with the first example with the initial interface configuration, as shown in Fig. 1, and the “high” total flow rate of  $Q=3 \times 10^{-2}$ . Figure 3 (left panels) shows the evolution of the initial fluid/fluid interface obtained through the numerical integration of Eq. (11) for a number of channel wavelengths. The temporal evolution is presented “toward” the viewer, that is, the initial configuration is at the rear of the plot and the profile just before the breakup is at the front. The flow is from right to left. All the solutions of the evolution equation shown were obtained with  $N=800$ , checks were made to make sure that this was sufficient to obtain mesh independence. Figure 3 (right panels) also exhibits the results computed with FLUENT, showing the channel’s wall (the upper line) and the interface profile just before the breakup (the lower line). The dimensionless times  $\tau$  corresponding to the final configuration are indicated below each plot.

Evidently, the evolution equation can follow the change in the interface shape until the latter touches the axis of the channel (defining the “breakup” moment), at which point the interface becomes discontinuous, and the solution for  $\kappa$  in Eq. (11) loses meaning. The final configurations are shown “just before the breakup,” meaning that further computation encounters a precipitous interface collapse. Such a precipitous terminal behavior of the computed solutions was also documented by Gauglitz and Radke.<sup>5</sup> For example, the final profile exhibited in Fig. 3(c) (left), shown at  $\tau=38$ , does not seem to be touching the centerline yet. However, continuing computations to just  $\tau=38.5$  already encounter a singularity, that is, a discontinuous interface and impossibility of obtaining a numerical solution. To validate the time scale of the evolution, the interface profiles obtained from the integration of Eq. (11) are compared with CFD at approximately the same spatial proximity to the axis of the channel, which involves a certain (but not large, due to a precipitous character of the late stages) degree of subjective judgment.

Figure 3(a) shows the evolution of the initial configuration that has the wavelength of the fastest-growing disturbance determined from the linear stability analysis. The wavelength is thus  $L=2^{3/2}\pi\kappa_0$ , or, keeping in mind that  $\kappa_0$  in this case is 0.5,  $\alpha \approx 0.450$ . The evolution of the interface proceeds in accordance with the pressure argument that led to the formulation of criterion (14). Driven by the excess pressure in the neck, the core fluid migrates into the crests of the channel and collects there, which leads to the eventual core pinch-off.

We wish to follow the change in the pattern of temporal evolution as the slope of the wall and the initial configuration (the value of  $\alpha$ ) is reduced from that of the maximum instability predicted by the linear stability analysis. Figure 3(b) presents the results for  $\alpha$  decreased by a factor of 2,  $\alpha=0.225$ , for the same initial profile. Although the pattern of the interface-shape evolution does not change dramatically, the snap-off is now achieved in a time that is about twice as great. This slower process is physically understood: the reduced slope means smaller gradients in capillary pressure, which consequently leads to a slower outflow of the fluid

from the neck. For the relatively high values of  $\alpha$  [Figs. 3(a) and 3(b)], the final interface shape is smooth and touches the centerline at one point; satellite drops are not produced.

Figure 3(c) illustrates the effects of further reduction in the slope. For the initial interface configuration in Fig. 1,  $R_{\min}$  in Eq. (14) is 0.3 and  $R_{\max}$  is 0.7. We now set  $\alpha$  in Eq. (14) to be one-tenth of its maximum value that, according to the pressure calculation, can lead to the breakup:  $\alpha=0.1(1/\pi\sqrt{R_{\min}R_{\max}})=0.0695$ . Figure 3(c) shows that the evolution of the interface is now even slower, and the breakup is achieved through the formation of “dimples” at the interface, which all develop from the originally “smooth” initial condition. As a result, as seen from the solution of the evolution equation [Fig. 3(c), left panel], the interface appears to touch the centerline at more than one point, forming one satellite drop. This is confirmed by FLUENT simulations. The drop is formed slightly downstream from the center of the neck between the two deepest “valleys” in the interface through which the film phase reaches the axis of the channel. The formation of the “waviness” of the profile is indicative of a nonlinear spatial-harmonic transformation due to the nonlinear character of the governing equation; as a result, the single wavelength of the initial configuration at time scales corresponding to the snap-off is not preserved. The much slower process seen in Fig. 3(c) lends itself for the development of rich nonlinear dynamics.

Note a slight “jaggedness” in the final profile presented in Fig. 3(c) (left). For purely aesthetic reasons in constructing a three-dimensional surface seen, only a limited number of the “topography” lines can be used; for the presentation purposes, this number has been kept at 70. Recall that the actual number  $N$  of grid points along the  $x$ -axis on the profiles has always been  $N=800$ , that is, the necessary numeric precision has been maintained.

The comparison of the interface shapes just before the breakup between the numerical solution of the evolution equation and the simulations by FLUENT (Fig. 3, left and right panels, respectively) shows a close similarity. The agreement in the total time to the breakup improves as the channel slope (parameter  $\alpha$ ) decreases. If we denote this time obtained from the evolution equation by  $\tau_{\text{bee}}$  and that from CFD modeling by  $\tau_{\text{bCFD}}$ , the ratio  $\tau_{\text{bee}}/\tau_{\text{bCFD}}=0.4, 0.5,$  and  $0.8$  for the cases in Figs. 3(a)–3(c), respectively. The pattern of the diminishing mismatch is to be expected, as the precision of the evolution model expressed in Eq. (11) increases with the decreasing slope. What comes as a surprise, though, is that the evolution equation turns out to be quite precise (relative to FLUENT) even for a relatively high  $\alpha$  of 0.450 [Fig. 3(a)].

It is interesting to estimate the absolute times needed for the full development of the core pinch-off. The dimensionless time  $\tau$  is measured in units of the characteristic time scale of the surface-tension-driven flow appearing in Eq. (1), equal to  $\mu_1^*R_T^*/\sigma^*$ . For the oil viscosity of 0.01 Pa s, surface tension of 0.040 N/m, and pore radius of 25  $\mu\text{m}$ , we obtain the time scale of approximately 6  $\mu\text{s}$ . The longest  $\tau$  observed in Fig. 3 is on the order of 40. The time to the breakup is thus on the order of 0.2 ms, or the fluid snap-off in this case happens instantly for the practical purposes.



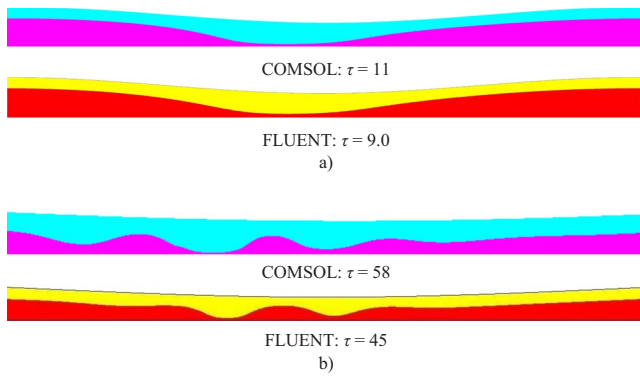


FIG. 4. (Color online) Comparison of the interface shapes near breakup computed with COMSOL and FLUENT. (a) The case of  $\alpha=0.450$ , corresponding to Fig. 3(a); (b) the case of  $\alpha=0.0695$ , corresponding to Fig. 3(c).

Figure 4 presents an example of comparison of interface shapes obtained with two independent CFD codes, FLUENT and COMSOL. COMSOL results are shown for the cases of Figs. 3(a) and 3(c) (right panels). The agreement is satisfactory in both the shapes of the interface and the times taken for the core fluid to break up.

Finally, condition (14) prohibits the formation of the breakup if the former is not satisfied, as then no pressure gradients will exist in the initial configuration that could set up the migration of the core fluid out of the neck. To verify if this predicted behavior is observed in the solutions of the evolution equation, we set  $\alpha$  just slightly above the threshold defined by Eq. (14),  $\alpha=1.05(1/\pi\sqrt{R_{\min}R_{\max}})=0.729$ . Figure 5 shows the temporal evolution of the initial profile in this case. As expected from the pressure argument, there is no continuous outflow of the core fluid from the constriction, and the initial profile equilibrates into a steady-state surface. The steady-state solutions are nearly identical in the evolution equation and FLUENT, and the geometric condition for the occurrence of the snap-off proves to be valid.

We now reduce the flow rate to  $Q=10^{-3}$ . Figure 6 recomputes the case of the slower and dynamically more complex evolution presented in Fig. 3(c) for this new value of  $Q$ . The comparison in the shape of the interface between the results of the integration of the evolution equation and those of FLUENT is very close; the computed times to the breakup are identical. If we compare Fig. 6 with Fig. 3(c), the reduction in the flow rate by a factor of 30 has not significantly affected the overall dynamics of the breakup process, except creating minor differences in the interface shape. One satel-

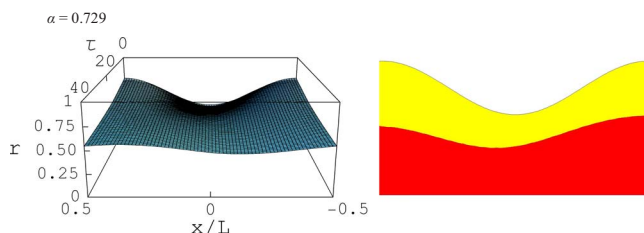


FIG. 5. (Color online) Evolution of the initial profile not satisfying the geometric condition (14) for the formation of the breakup in the neck:  $\alpha=0.729$ .  $Q=3\times 10^{-2}$  and  $\mu_1/\mu_2=10$  as in Fig. 3.

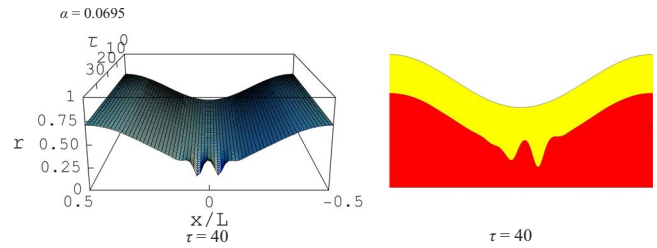


FIG. 6. (Color online) Evolution of the initial profile with  $Q=10^{-3}$ . All other conditions are as in Fig. 3(c).

lite drop is still shed, and it is closer to the center of the constriction because of the slower flow.

Note that the linear stability treatment of the core-annular flow in straight cylindrical channels has shown windows of finite Reynolds numbers in which the Plateau-Rayleigh instability is suppressed, in case of  $\mu_1 > \mu_2$  (the core more viscous than the film).<sup>20</sup> It is important to recognize in the context of our study that at small Re, the flow is unstable for long wavelengths (that is, satisfying the condition  $L > 2\pi R$  for the Plateau-Rayleigh instability) for both  $\mu_1 > \mu_2$  (considered so far) and  $\mu_1 < \mu_2$ .<sup>20,21</sup> To check the consistency with the latter prediction, we resimulate the scenario of Fig. 6 with the viscosity ratio reversed, that is  $\mu_1/\mu_2=0.1$ . The result is depicted in Fig. 7. The instability is preserved with the same major features of the solution as in Fig. 6, except that the breakup process has become much slower due to a greatly increased viscosity of the film. There is an excellent match in the final interface shapes between the evolution model and FLUENT. The ratio of  $\tau_{\text{bee}}/\tau_{\text{bCFD}}$  is 0.8.

To illustrate the generic character of the inferences regarding the character of the evolution of the interface, we consider a different initial annulus thickness equal to one-half of that in Fig. 1. Figure 8 shows the new initial configuration. We solve the evolution equation for the same scenario as in Fig. 3(c), one with the richer nonlinear dynamics, which has the slope of one-tenth of the maximum value that can lead to the breakup:  $\alpha=0.1(1/\pi\sqrt{R_{\min}R_{\max}})=0.0515$  ( $R_{\min}=0.45$  and  $R_{\max}=0.85$ ). The temporal evolution for the high  $Q$  of  $3\times 10^{-2}$  is presented in Fig. 9. The evolution of the interface proceeds similarly through the formation of short-wave disturbances (dimples) before the snap-off; however, for this scenario, the satellite drop is not generated [cf. Fig. 3(c)]. The collar of the annulus fluid across the

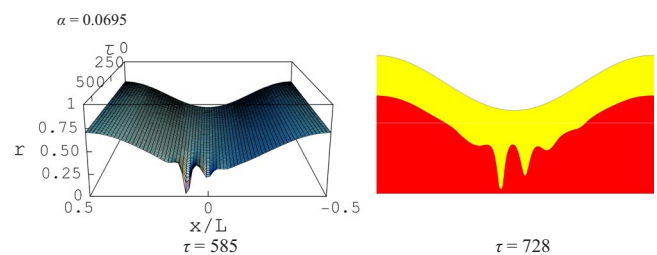


FIG. 7. (Color online) Evolution of the initial profile with  $\mu_1/\mu_2=0.1$ . All other conditions are as in Fig. 6.

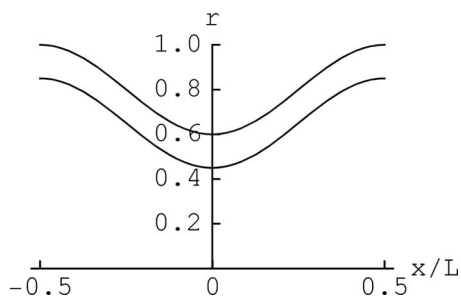


FIG. 8. Geometry of the case with the reduced initial film thickness.

channel is produced through one deep and sharp “valley” in the interface, clearly seen in both the evolution-equation and FLUENT results (Fig. 9, left and right panels, respectively). Both the interface shapes and the times to breakup compare very favorably ( $\tau_{\text{bee}}/\tau_{\text{bCFD}}=0.9$ ) between the evolution equation and FLUENT. As one could expect, the process has become much slower (the final times  $\tau$  are on the order of 400) because the collar now has to develop through a thicker viscous core.

#### IV. CONCLUSIONS

We have derived an evolution equation describing the core-annular temporal dynamics for arbitrary fluid viscosities in axisymmetric capillary channels with imposed base flow, including the possibility of the core pinch-off.

In the case of the surface-tension-driven flow, for the sinusoidal pores, a purely geometric condition (14) exists that defines the exceedance of capillary pressure in the neck of the constriction relative to the crest of the profile; it thus ensures the outflow of the core fluid out of the neck toward the crests of the initial configuration of the fluid/fluid interface. Inequality (14) thus establishes the geometric condition for the development of the fluid breakup.<sup>15</sup> Numerical simulations with both the evolution equation and CFD codes demonstrate that this pattern, expected solely from the capillary-pressure analysis, indeed takes place in the nonlinear dynamics of the interface.

When condition (14) is satisfied, the curvature of the profile is sufficient to set up pressure gradients that lead to the snap-off in relatively short absolute times for the

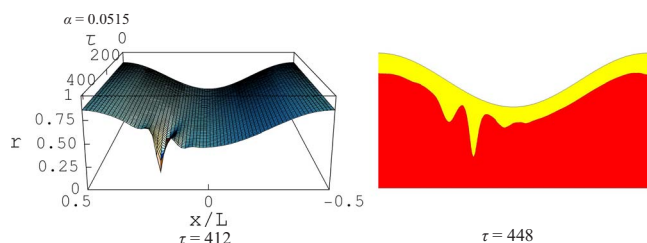


FIG. 9. (Color online) Evolution of the initial profile with the slope of one-tenth of the maximum value that can lead to the breakup for the reduced initial film thickness:  $\alpha=0.0515$ .  $Q=3 \times 10^{-2}$  and  $\mu_1/\mu_2=10$  as in Fig. 3.

examples considered. The following patterns emerge. When the slopes of the channel wall and the interface are relatively large, producing larger pressure gradients and shorter evolution times, the interface shapes tend to remain smooth and collapse at single points on the channel axis. No satellite droplets are produced. However, with the decreasing slopes and rising evolution times, the waviness of the profiles is developed from the initial configuration through a nonlinear interaction of growing disturbances. The snap-off in such a case tends to be achieved through growing dimples that may touch the centerline at several points, forming satellite drops. Instabilities develop for the cases of both  $\mu_1 > \mu_2$  and  $\mu_1 < \mu_2$ , agreeing with the results of earlier linear stability analyses. Variation in the flow rate does not seem to significantly alter this pattern.

In the context of the nonlinear dynamics observed, it should be noted that asymptotic analyses of the core-annular flow in straight tubes in the limit of small film thickness have led to the Kuramoto–Sivashinsky equation, e.g., Ref. 9. Numerical studies of this equation have documented similar processes of appearance, growth, sharpening, and nonlinear interaction of disturbances at extraneous frequencies not coinciding with that of the fastest growing wave of the linear stability analysis. However, as noted in Sec. I, such asymptotic models have a limited practical value as they have been unable to predict the formation of liquid bridges across the tube.

Instabilities of the interface do not occur if there is no initial pressure gradient that would enable migration of the core fluid from the neck, that is, geometric condition (14) is not satisfied. In that case, the evolution of the interface proceeds toward a quick equilibration of the initial configuration toward steady-state flow.

The evolution equation is asymptotic in the sense that it has been derived with the small-slope assumption (a sufficiently small parameter  $\alpha$ ). The results obtained through the numerical integration of the evolution equation have been validated against two numerically independent, fully dynamic CFD codes for  $\alpha$ 's changing from nearly one downward. As one could anticipate, the validations showed an improving match between the evolution equation and CFD with decreasing  $\alpha$ . The comparisons have also demonstrated that the evolution equation reasonably well describes interface shapes and times to the breakup (within a factor of 2 or so) even for the slope parameter  $\alpha$  approaching the value of 1.

The evolution-equation approach proves to be an efficient way to distinguish between different physical scenarios and inexpensively compute the dynamics of a free fluid/fluid interface.

#### ACKNOWLEDGMENTS

This work was funded by the National Science Foundation and the Petroleum Research Fund. Acknowledgment is made to the donors of the American Chemical Society's Petroleum Research Fund for support of this research. We are

grateful to D. Vigil for the help in the course of the study. We also thank the two anonymous reviewers for the valuable suggestions.

- <sup>1</sup>L. D. Landau and E. M. Lifshitz, *Fluid Mechanics* (Pergamon, New York, 1975).
- <sup>2</sup>R. W. Atherton and G. M. Homsy, "On the derivation of evolution equations for interfacial waves," *Chem. Eng. Commun.* **2**, 57 (1976).
- <sup>3</sup>P. S. Hammond, "Nonlinear adjustment of a thin annular film of viscous fluid surrounding a thread of another within a circular cylindrical pipe," *J. Fluid Mech.* **137**, 363 (1983).
- <sup>4</sup>P. A. Gauglitz and C. J. Radke, "An extended evolution equation for liquid film breakup in cylindrical capillaries," *Chem. Eng. Sci.* **43**, 1457 (1988).
- <sup>5</sup>P. A. Gauglitz and C. J. Radke, "The dynamics of liquid film breakup in constricted cylindrical capillaries," *J. Colloid Interface Sci.* **134**, 14 (1990).
- <sup>6</sup>T. M. Tsai and M. J. Miksis, "Dynamics of a drop in a constricted capillary tube," *J. Fluid Mech.* **274**, 197 (1994).
- <sup>7</sup>C. Kouris and J. Tsamopoulos, "Core-annular flow in a periodically constricted circular tube. Part 2. Nonlinear dynamics," *J. Fluid Mech.* **470**, 181 (2002).
- <sup>8</sup>D. T. Papageorgiou, C. Maldarelli, and D. S. Rumschitzki, "Nonlinear interfacial stability of core-annular film flows," *Phys. Fluids A* **2**, 340 (1990).
- <sup>9</sup>V. Kerchman, "Strongly nonlinear interfacial dynamics in core-annular flows," *J. Fluid Mech.* **290**, 131 (1995).
- <sup>10</sup>H.-H. Wei and D. S. Rumschitzki, "The linear stability of a core-annular flow in an asymptotically corrugated tube," *J. Fluid Mech.* **466**, 113 (2002).
- <sup>11</sup>H.-H. Wei and D. S. Rumschitzki, "The weakly nonlinear interfacial stability of a core-annular flow in a corrugated tube," *J. Fluid Mech.* **466**, 149 (2002).
- <sup>12</sup>J. C. Melrose and C. F. Brandner, "Role of capillary forces in determining microscopic displacement efficiency for oil recovery by waterflooding," *J. Can. Pet. Technol.* October–December, 54 (1974).
- <sup>13</sup>S. Middleman, *Modeling Axisymmetric Flows* (Academic, New York, 1995).
- <sup>14</sup>P.-G. De Gennes, F. Brochard-Wyart, and D. Quéré, *Capillarity and Wetting Phenomena* (Springer, New York, 2004).
- <sup>15</sup>I. A. Beresnev, W. Li, and R. D. Vigil, "Condition for break-up of non-wetting fluids in sinusoidally constricted capillary channels," *Transp. Porous Media* **80**, 581 (2009).
- <sup>16</sup>C. Kouris and J. Tsamopoulos, "Concentric core-annular flow in a circular tube of slowly varying cross-section," *Chem. Eng. Sci.* **55**, 5509 (2000).
- <sup>17</sup>F. P. Bretherton, "The motion of long bubbles in tubes," *J. Fluid Mech.* **10**, 166 (1961).
- <sup>18</sup>F. M. White, *Viscous Fluid Flow*, 3rd ed. (McGraw-Hill, New York, 2006).
- <sup>19</sup>J. Bear, *Dynamics of Fluids in Porous Media* (Dover, New York, 1988).
- <sup>20</sup>K. Preziosi, K. Chen, and D. D. Joseph, "Lubricated pipelines: Stability of flow," *J. Fluid Mech.* **201**, 323 (1989).
- <sup>21</sup>H. H. Hu and D. D. Joseph, "Lubricated pipelines: Stability of core-annular flow. Part 2," *J. Fluid Mech.* **205**, 359 (1989).